Demosaicking of Noisy Bayer-Sampled Color Images With Least-Squares Luma-Chroma Demultiplexing and Noise Level Estimation

Gwanggil Jeon, *Member, IEEE*, and Eric Dubois, *Fellow, IEEE*

Abstract—This paper adapts the least-squares luma-chroma demultiplexing (LSLCD) demosaicking method to noisy Bayer color filter array (CFA) images. A model is presented for the noise in white-balanced gamma-corrected CFA images. A method to estimate the noise level in each of the red, green, and blue color channels is then developed. Based on the estimated noise parameters, one of a finite set of configurations adapted to a particular level of noise is selected to demosaic the noisy data. The noise-adaptive demosaicking scheme is called LSLCD with noise estimation (LSLCD-NE). Experimental results demonstrate state-of-the-art performance over a wide range of noise levels, with low computational complexity. Many results with several algorithms, noise levels, and images are presented on our companion web site along with software to allow reproduction of our results.

Index Terms—Bayer sampling, color filter array, demosaicking, noise estimation, noise model, noise reduction.

I. INTRODUCTION

MOST DIGITAL cameras acquire color images with the use of a color filter array (CFA), whereby only one color component is measured at each spatial location of the sensor. The most popular CFA pattern in current use continues to be the one due to Bayer. The process of reconstructing three color components at each point of the spatial sampling structure is known as *demosaicking*. A large number of methods have been proposed to carry out this demosaicking process; a recent survey can be found in [1]. One successful class of methods is based on a frequency-domain interpretation of the spatial multiplexing of red, green and blue components; it has been termed the method of luma-chroma demultiplexing in [2]. Coupled with a least-squares methodology for designing the associated filters, it was called least-squares luma-chroma demultiplexing (LSLCD), a term we adopt in this paper. The method was shown in [2] to give a state-of-the-art quality/complexity tradeoff for essentially noise-free Bayer CFA images. However, noise introduced by the acquisition process

is always present in the CFA images acquired by digital cameras and it can seriously affect demosaicking performance. Thus, the processing of raw camera images requires both demosaicking and denoising processes. This paper addresses the problem of accounting for noise in LSLCD demosaicking.

Many demosaicking methods have been proposed (e.g., [2]–[7]), and their performance has been established on noise-free CFAs. To make the system more realistic, many recent papers have described demosaicking/denoising methods for noisy CFA signals [8]–[16]. Their purpose is to reduce the noise while maintaining significant signal details as much as possible. There are two main issues to consider in a demosaicking/denoising system. The first is the noise model to be used. The noise introduced at the sensor is signal dependent noise [17] and some papers have taken this into account [8], [10], [18]. However, as we argue in section II of this paper, it is reasonable to model the noise in the *white-balanced, gamma-corrected* signal as signal-independent white Gaussian noise, but with different variances in the different color channels. The second issue is the structure of the demosaicking/denoising system. It is possible to first perform denoising of the CFA image followed by demosaicking [14], [15], or to first perform demosaicking followed by denoising. Several drawbacks of such approaches were reported in [11], [12]. Thus, it should be better to jointly perform demosaicking and denoising, the approach we take here.

We briefly review the methods that have been proposed for joint demosaicking and denoising. Zhang *et al.* presented a method which estimates the color differences with a minimum MSE technique that exploits both spectral and spatial correlations to simultaneously eliminate sensor noise and reconstruction error [9]. Paliy *et al.* presented an efficient spatially adaptive nonlinear filter by utilizing a local polynomial approximation to eliminate the demosaicking noise generated in the demosaicking process. Later they used this method to suppress noise and demosaic the CFA signal [10]. Menon and Calvagno utilized a space-varying filtering and autocorrelation evaluation approach [12]. In [11], Zhang *et al.* used the approach of principle component analysis to analyze the local structure of each CFA variable block, which includes color components from different channels. In [13], Condat proposed filters for denoising green/magenta and red/blue chrominance and used BM3D [19] to denoise the luminance component.

In this paper, we present a noise-adaptive demosaicking system based on LSLCD, where training of the filters in the

G. Jeon is with the Department of Embedded Systems Engineering, University of Incheon, Incheon 406-772, Korea (e-mail: gjeon@incheon.ac.kr).

E. Dubois is with the School of Electrical Engineering and Computer Science, University of Ottawa, Ottawa, ON K1N 6N5, Canada (e-mail: edubois@uottawa.ca).

system is done on noisy signals obtained by artificially adding noise according to our model to the images in a training set. Different noise levels are added in the different color channels according to the camera model. A different LSLCD system is designed for each of a discrete set of noise levels. To select which set of filters should be used, we must estimate the noise level in the CFA signal, a problem which has not received attention in the literature. To this end, we have adapted the noise estimation method of Amer and Dubois [20] to the problem of estimating the noise levels in the three channels of a Bayer CFA, and use the result to select one of the pre-designed filter sets for demosaicking. We call the resulting system LSLCE with noise estimation, or LSLCD-NE and show in this paper that it gives state-of-the-art performance for this problem over a wide range of noise levels.

The remainder of this paper is organized as follows. In Section II, we present our model for the formation of the noisy CFA signal after white balance and gamma correction. Section III reviews the LSLCD system, showing how it can be used with noisy data, and how the BM3D scheme of [19] can be integrated with it. The adaptation of the noise estimator of [20] to noisy CFA signals is presented in Section IV. Then Section V shows how the estimated noise parameters are used to select the filters for the LSLCD-NE algorithm. Experimental evaluations and comparisons are given in Section VI. A representative set of demosaicked images and software to replicate the results can be found on our associated web page [21]. Conclusions are drawn in Section VII.

II. FORMATION OF THE NOISY CFA IMAGE

Random noise is introduced into the CFA image at the level of the sensor. There are typically two sources of noise: Poisson distributed noise generated in the process of converting photons to electrons (shot noise), and electronic amplifier noise [18]. The image at the output of the Bayer CFA sensor in the noise free case can be modeled as [22]

$$f_{raw}[\mathbf{x}] = \int_{\lambda_{min}}^{\lambda_{max}} \int_{\mathbb{R}^2} f(\mathbf{x} - \mathbf{s}, \lambda) h_a(\mathbf{s}) d\mathbf{s}\, c_i(\lambda) d\lambda,$$
$$\mathbf{x} \in \Psi_i, i = 1, 2, 3. \quad (1)$$

In this expression, Ψ_i is the sampling structure for the ith sensor class, where $i = 1, 2, 3$ correspond to R, G and B respectively. The functions $c_i(\lambda)$ represent the spectral sensitivities of the red, green and blue filters placed over the sensor elements. Typical examples that we have used in our work are shown in Fig. 5.1 of [23]. The function $h_a(\mathbf{s})$ is the camera aperture and $f(\mathbf{x}, \lambda)$ is the spectral irradiance that would be projected at position $\mathbf{x}$ by an ideal (pinhole) optical system.

This signal is corrupted by noise as described above to yield the noisy sensor output

$$f_{rawn}[\mathbf{x}] = f_{raw}[\mathbf{x}] + v[\mathbf{x}], \quad (2)$$

where $v[\mathbf{x}]$ is a zero-mean random noise whose statistics we assume do not depend on $\mathbf{x}$ but which generally depend on the value of f_{raw}. A typical model for digital cameras is that v is the sum of two independent noise terms, where one is signal

independent and the other has a variance proportional to the signal value [17]. Such a model could be formulated as

$$f_{rawn}[\mathbf{x}] = f_{raw}[\mathbf{x}] + \sqrt{m_0} v_1[\mathbf{x}] + \sqrt{m_1 f_{raw}[\mathbf{x}]} v_2[\mathbf{x}], \quad (3)$$

where v_1 and v_2 are independent zero-mean, unit variance white Gaussian noise processes, and m_0 and m_1 are parameters that describe the noise level. (See [24] for a similar, more elaborate model that accounts for clipping.) In this model, the variance of the noise, given f_{raw}, is $E[v^2|f_{raw}] = m_0 + m_1 f_{raw}$.

This noise will impact all subsequent image processing operations and should be accounted for when optimizing these operations. Examples of such operations are white balancing, color space conversion (from the camera color space to CIE color space), gamma correction, denoising, and of course demosaicking. These operations can be carried out separately in some particular order, or they can be integrated to give the best overall solution. In this paper, we neglect the color space conversion and assume that the noise-free values f_{raw} represent sRGB tristimulus values on the respective R, G, B sampling structures. We assume that white balance is first carried out, followed by gamma correction, and then joint demosaicking/denoising. Thus, we wish to model the noise in the white-balanced, gamma-corrected signal.

To achieve white balance, the individual raw channels are multiplied by constants α_i so that the response to a reference white spectrum is 1.0 in each channel. Examples of this calculation are given in section 5.2 of [23] for Canon 10D and Nikon D76 data from [25]. Finally, the signal values pass through a gamma-correction operation $g^{-1}(\cdot)$, such as sRGB gamma correction (e.g., eq. (5.11) in [23]). Thus, the white-balanced, gamma-corrected CFA signal can be modeled as

$$f'_{\text{CFAN}}[\mathbf{x}] = g^{-1}(\alpha[\mathbf{x}] f_{raw}[\mathbf{x}] + \alpha[\mathbf{x}] v[\mathbf{x}]), \quad (4)$$

where $\alpha[\mathbf{x}] = \alpha_i$ for $\mathbf{x} \in \Psi_i$, whereas the ideal signal is

$$f'_{\text{CFA}}[\mathbf{x}] = g^{-1}(\alpha[\mathbf{x}] f_{raw}[\mathbf{x}]). \quad (5)$$

If we write

$$f'_{\text{CFAN}}[\mathbf{x}] = f'_{\text{CFA}}[\mathbf{x}] + v'[\mathbf{x}] \quad (6)$$

we would like to model the noise $v'[\mathbf{x}]$ in each channel Ψ_i.

In this paper, we propose to model the noise in each channel of the gamma-corrected signal as white Gaussian noise with variances σ_R^2, σ_G^2 and σ_B^2 respectively, that are essentially determined by the gains needed to achieve white balance. The motivation is as follows. Suppose that m_0 is small and can be considered negligible (as in modern high-quality cameras), and that the gamma correction is simply a power-law operation $g^{-1}(f) = f^{1/\gamma}$, which is a reasonable approximation. For example, sRGB gamma correction can be very closely modeled by such a power law with $\gamma = 2.2$ [26].
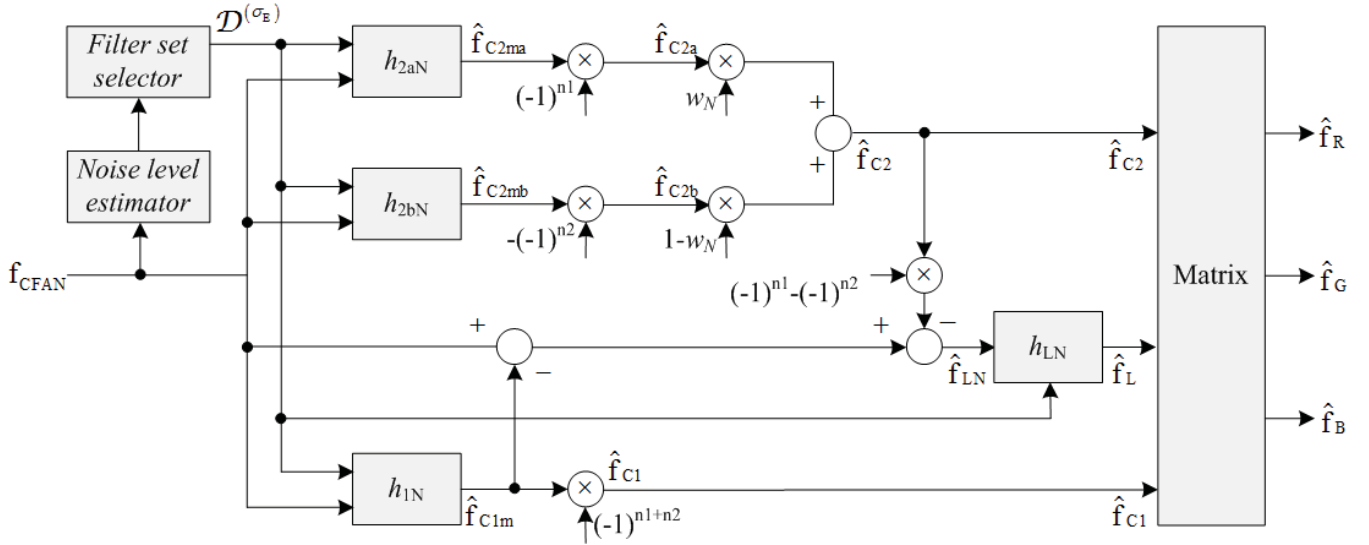
Fig. 1.   Block diagram of the proposed LSLCD-NE system.

Then, at any particular point $\mathbf{x}$

$$f_{rawn} = f_{raw} + \sqrt{m_1 f_{raw}}\, v_2$$

$$\frac{f_{rawn}}{f_{raw}} = 1 + \sqrt{\frac{m_1}{f_{raw}}}\, v_2$$

$$\left(\frac{f_{rawn}}{f_{raw}}\right)^{1/\gamma} = \left(1 + \sqrt{\frac{m_1}{f_{raw}}}\, v_2\right)^{1/\gamma}$$

$$\approx 1 + \frac{1}{\gamma}\sqrt{\frac{m_1}{f_{raw}}}\, v_2, \qquad (7)$$

where we are keeping the first two terms of the Taylor expansion of $(1 + a)^{1/\gamma}$ for small a. It follows that (taking the approximation as equality)

$$(f_{rawn})^{1/\gamma} = (f_{raw})^{1/\gamma} + \frac{1}{\gamma}\sqrt{m_1}\, v_2 f_{raw}^{(2-\gamma)/2\gamma}$$

$$(\alpha f_{rawn})^{1/\gamma} = (\alpha f_{raw})^{1/\gamma} + \frac{1}{\gamma}\sqrt{m_1}\, \alpha^{1/\gamma} v_2 f_{raw}^{(2-\gamma)/2\gamma}$$

$$v'[\mathbf{x}] = \frac{1}{\gamma}\sqrt{m_1}\, \alpha^{1/\gamma} v_2[\mathbf{x}] (f_{raw}[\mathbf{x}])^{(2-\gamma)/2\gamma}. \qquad (8)$$

We see that if $\gamma = 2$, $v'[\mathbf{x}]$ is signal independent. If $\gamma = 2.2$, then v' is proportional to $f_{raw}^{-0.045}$, which is nearly signal independent. In a simulation of sRGB gamma correction on uniformly distributed data, the PSNR in ten amplitude bins over the signal range varied from about 33.9 dB to 36.8 dB, whereas it ranges from 43.1 dB to 30.7 dB in the non-gamma-corrected signal. Thus, it is reasonable to model noise in the white-balanced gamma-corrected signal as signal-independent white Gaussian noise, but with channel-dependent variances

$$\sigma_R^2 : \sigma_G^2 : \sigma_B^2 = \alpha_R : \alpha_G : \alpha_B. \qquad (9)$$

For the Canon 10D as described in [23], we have $\alpha_R : \alpha_G : \alpha_B = 1.86 : 0.69 : 1.0$ and for the Nikon D70, $\alpha_R : \alpha_G : \alpha_B = 1.72 : 0.68 : 1.0$.

III. LSLCD DEMOSAICKING OF NOISY BAYER CFA SIGNALS

We have shown in [2] how a noise-free Bayer CFA signal can be demosaicked using luma-chroma demultiplexing with least-squares filters. Specifically, we can express the CFA signal as

$$\begin{aligned} f_{CFA}[n_1, n_2] &= f_L[n_1, n_2] + f_{C1}[n_1, n_2] e^{j\pi(n_1+n_2)} \\ &\quad + f_{C2}[n_1, n_2]\left(e^{j\pi n_1} - e^{j\pi n_2}\right) \\ &\triangleq f_L[n_1, n_2] + f_{C1m}[n_1, n_2] \\ &\quad + f_{C2ma}[n_1, n_2] + f_{C2mb}[n_1, n_2], \end{aligned} \qquad (10)$$

with Fourier transform

$$\begin{aligned} F_{CFA}(u, v) &= F_L(u, v) + F_{C1}(u - 0.5, v - 0.5) \\ &\quad + F_{C2}(u - 0.5, v) - F_{C2}(u, v - 0.5), \end{aligned} \qquad (11)$$

where frequencies are expressed in c/px. The luma and chroma components are related to the RGB components by the matrix transformation

$$\begin{bmatrix} f_L \\ f_{C1} \\ f_{C2} \end{bmatrix} = \begin{bmatrix} \frac{1}{4} & \frac{1}{2} & \frac{1}{4} \\ -\frac{1}{4} & \frac{1}{2} & -\frac{1}{4} \\ -\frac{1}{4} & 0 & \frac{1}{4} \end{bmatrix} \begin{bmatrix} f_R \\ f_G \\ f_B \end{bmatrix}. \qquad (12)$$

Demosaicking is accomplished by extracting estimates of f_{C1} and f_{C2} using band-pass filters h_1, h_{2a}, and h_{2b}, followed by demodulation. A key ingredient to the success of that algorithm in an adaptive combination of the two independent modulated versions of f_{C2} at frequencies (0.5,0.0) and (0.0,0.5). The luma component is obtained by subtracting the estimated modulated chroma components from the CFA signal, and the estimated R, G, B components are obtained by applying the inverse of Eq. (12). The system is defined by the filters h_1, h_{2a} and h_{2b}, which were obtained in [2] using a least-squares criterion on a suitable training set. That algorithm, referred to as least-squares luma-chroma demultiplexing (LSLCD) is summarized in Fig. 1 of [2].
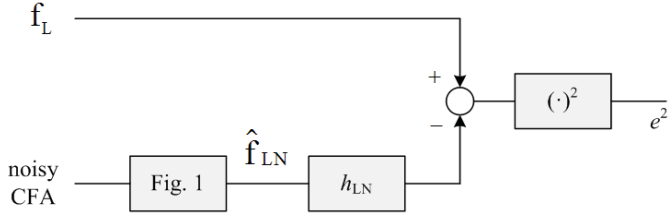
Fig. 2. Block diagram of the setup for training filter h_{LN} for noisy luminance component.

In this paper, we adapt the LSLCD approach to demosaicking noisy Bayer CFA signals. As described in Section II, we assume that the three measured components are corrupted with additive white Gaussian noise, but with different (unknown) variances. Depending on our knowledge of the acquisition system, the ratio of the variances may or may not be known, but we may assume that they are approximately as given in Section II for the Canon 10D and Nikon D70 cameras. The demosaicking algorithm is essentially the same as in [2], but the least-squares filters are trained on noisy signals. In the training phase, noise is added to the gamma-corrected R, G, B components with the given ratio of variances. Filters are then designed to minimize the squared error between the filtered noisy CFA signals and the corresponding noise-free modulated chroma components. The approach is identical to that of [2] except that filters are applied to simulated noisy CFA signals. Note that the noise in the modulated chroma components is a mixture of the different RGB noise terms, but this is captured automatically by the least-squares approach.

Since the real noise level is variable and unknown, we have designed least-squares filters for P different levels of noise, where the noise variances in R, G, and B are in a given predefined ratio. In this way, we design P different demosaicking systems, each adapted to a different noise level. Our approach is to estimate the noise level from the CFA signal, and then choose the best adapted system from among the P candidates, as shown in Fig. 1. We note that the adaptive combining of $\hat{f}_{C2a}$ and $\hat{f}_{C2b}$ is done exactly as in [2]. One notable difference is that the luma signal estimate obtained by subtracting the estimated modulated chroma signals from the noisy CFA signal will contain noise in the luma band. This noise can be reduced using any denoising algorithm for gray-scale images. We have done this using another least-squares filter h_{LN} that minimizes the squared error between the filtered noisy luma estimate and the noise-free luma on the training set, as shown in Fig. 2. We have also used the BM3D noise reduction filter of Dabov et al. [19], as suggested by Condat [13].

Fig. 3 illustrates a typical set of filters obtained with this algorithm. Fig. 3(a)–(d) shows filters designed when there is no added noise, while Fig. 3(e)–(h) shows the filters obtained for $\sigma_A = 10$. The effect of the noise on the filter design is quite evident.

IV. ESTIMATING NOISE LEVEL IN R, G, B CHANNELS

To select the appropriate set of trained filters, we need to know the noise level in the three channels of the CFA signal.

Although there have been many methods developed for noise level estimation in single-channel images, there has been little work on this problem for CFA signals. We have experimented with various techniques for noise level estimation and found that the method of Amer and Dubois [20] is most suitable for our problem. This section shows how the method of [20] has been adapted for CFA images.

Since we only deal with gamma-corrected images in this paper, the prime notation of section II is dropped. Thus, we assume

$$f_{CFAN}[n_1, n_2] = f_{CFA}[n_1, n_2] + v[n_1, n_2] \qquad (13)$$

where $v[n_1, n_2]$ is independent white Gaussian noise with variance σ_i^2 in the ith channel ($[n_1, n_2] \in \Psi_i$). We have tested our noise estimation methods on two standard image data sets with added noise: the 768×512 Kodak images (KO), and the data set of 720×540 images made available by L. Condat [27] (LC).

A. Basic Noise Estimation Algorithm

To adapt the noise estimation of [20] to CFA images, we partition the image into four rectangularly sampled subimages R, G_1, G_2, and B, corresponding to the four phases of the Bayer pattern. The proposed method estimates the global image noise variance from the variances of a set of blocks within the subimages classified as the most intensity-homogeneous blocks (IHB).

This method selects IHBs in a subimage by rejecting blocks with line structure, using the masks of [20] to detect line structures. The noise level estimation method consists of two parts: (1) detection of IHBs, (2) calculating $\sigma_i = \sqrt{\alpha_i}\sigma_A$ for color $i \in \{R, G, B\}$ of the selected blocks. For each subimage, we define square $\omega \times \omega$ blocks $B_{kl}^{(j)}$, centered at each location (k, l) in the subimage, $j \in \{R, G_1, G_2, B\}$. We denote the sample mean and sample variance for each block by $\mu_{B_{kl}^{(j)}}$ and $\sigma^2_{B_{kl}^{(j)}}$. The assumption is that for the most homogeneous blocks in the image, $\mu_{B_{kl}^{(j)}}$ represents the signal value and the variance $\sigma^2_{B_{kl}^{(j)}}$ can be attributed to the noise in the corresponding channel, and is a good estimate of the noise variance in that channel.

To determine if a block can be classified as an IHB, we need to calculate a homogeneity measure, $\xi_{B_{kl}^{(j)}}$. Assume we have eight directional homogeneity measures from eight edge directions (masks as shown in Fig. 4 for $\omega = 5$), where $\zeta^{(m)}_{B_{kl}^{(j)}}$ is the absolute value of the output of a one-dimensional high pass filter applied on mask contour m as shown in Fig. 4, evaluated at the center of the block. We assume that blocks with the smallest sum of all directional homogeneity measures, $\xi_{B_{kl}^{(j)}} = \sum_{1 \leq m \leq 8} \zeta^{(m)}_{B_{kl}^{(j)}}$, may be identified as IHBs. Several combinations of configurations can be made for determining IHBs. They can be determined by (1) window size ω (ω is an odd number, $\omega \geq 3$), (2) skipping parameter τ to reduce the computational cost (horizontally and vertically skipping each τth pixel in an image), (3) high pass filter (HPF) design ($f_{HP}^3 = [-1\ 2\ -1]$,
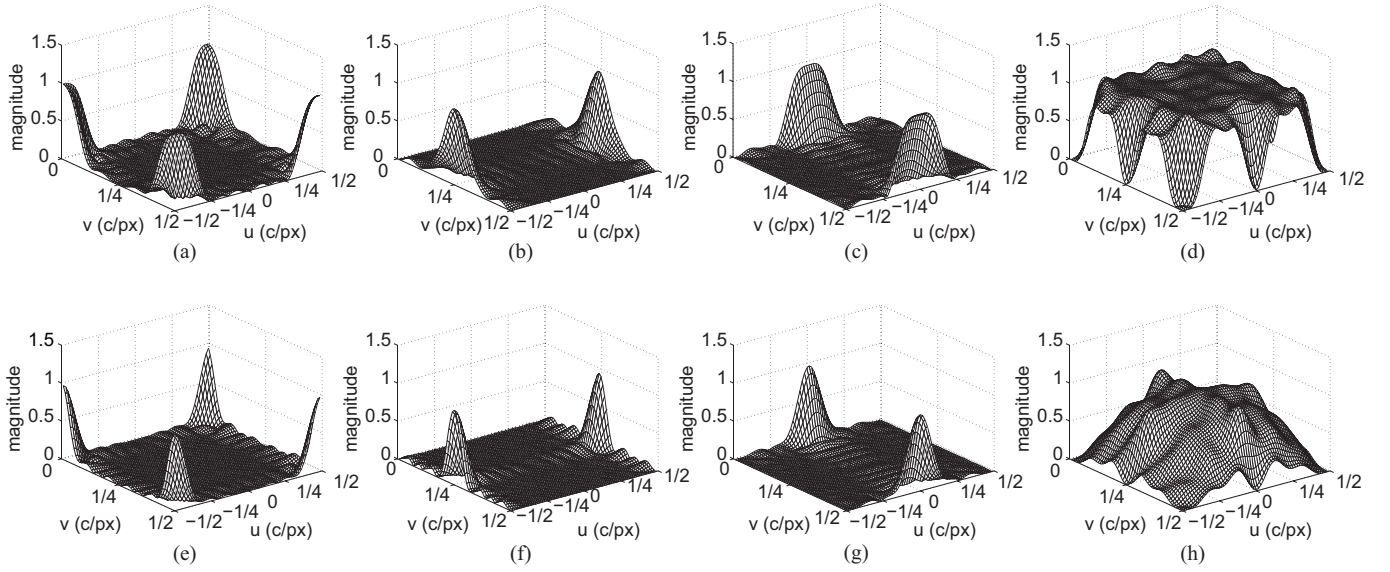
Fig. 3.   Perspective view of frequency responses of typical 11×11 sized filters. (a) h_1, (b) h_{2a}, (c) h_{2b}, (d) h_L for noise-free CFA. (e) h_{1N}, (f) h_{2aN}, (g) h_{2bN}, and (h) h_{LN} for noisy CFA ($\sigma_A = 10$).
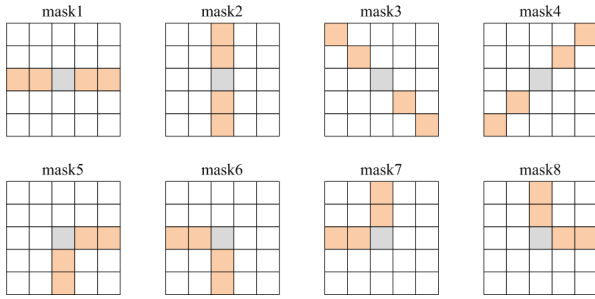

Fig. 4.   Direction of the homogeneity analyzer when $\omega = 5$.

$f_{HP}^5 = [-1 \ -1 \ 4 \ -1 \ -1]$, filter size is $1 \times \omega$). The selected configuration for our application has been determined empirically as $[\omega, \tau, HPF] = [5, 3, f_{HP}^5]$. Figure 4 shows the homogeneity analyzer, where $f_{HP}^5 = [-1 \ -1 \ 4 \ -1 \ -1]$ is chosen as the high pass filter which measures the degree of homogeneity in the eight different directions.

The blocks with lowest sum of all homogeneity measures are assumed to be close to the ideal IHB. However, deciding the noise level using just one IHB is not reliable. Therefore we use three blocks in each subimage to estimate the corresponding unknown noise variance. Let $V^{(j)}$ be the set of locations of the centers of three blocks in subimage j with the lowest aggregate homogeneity measure (aside from the lowest one). The corresponding sample variances are $\sigma_{B_{kl}^{(j)}}^2, (k, l) \in V^{(j)}$ for $j \in \{R, G_1, G_2, B\}$, and the estimate of the variance for each phase is

$$\sigma_{e,j}^2 = \frac{1}{3} \sum_{(k,l) \in V^{(j)}} \sigma_{B_{kl}^{(j)}}^2. \tag{14}$$

If we know the exact ratio of $\alpha_R : \alpha_G : \alpha_B$ that was used to obtain f_{CFAN}, we select $\sigma_e^{T\alpha}$ as,

$$\sigma_e^{T\alpha} = \text{median}\left[\frac{\sigma_{e,R}}{\sqrt{\alpha_R}}, \frac{\sigma_{e,G_1}}{\sqrt{\alpha_G}}, \frac{\sigma_{e,G_2}}{\sqrt{\alpha_G}}, \frac{\sigma_{e,B}}{\sqrt{\alpha_B}}\right] \tag{15}$$

where $T\alpha$ stands for *true alpha ratio*, which means we apply the known alpha values for estimating the noise standard deviation.

However, as we describe in Section II, the ratio $\alpha_R : \alpha_G : \alpha_B$ can be different depending on camera models. Therefore we may have to estimate the $\alpha_R : \alpha_G : \alpha_B$ ratio first before we determine σ_e. From Eq. 9 we know $\sigma_R^2 : \sigma_G^2 : \sigma_B^2 = \alpha_R : \alpha_G : \alpha_B$, so we assume $\frac{\sigma_{e,R}}{\sqrt{\alpha_R}} \approx \frac{\sigma_{e,G_1}}{\sqrt{\alpha_G}} \approx \frac{\sigma_{e,G_2}}{\sqrt{\alpha_G}} \approx \frac{\sigma_{e,B}}{\sqrt{\alpha_B}}$. If we arbitrarily set $\alpha_B = 1$, then α_R and α_G are calculated as

$$\left(\frac{\sigma_{e,R}}{\sigma_{e,B}}\right)^2 : \frac{\sigma_{e,G_1}^2 + \sigma_{e,G_2}^2}{2\sigma_{e,B}^2} : 1 \approx \alpha_R : \alpha_G : \alpha_B, \tag{16}$$

and $\sigma_e^{E\alpha}$ is calculated as Eq. 15. Here $E\alpha$ stands for *estimated alpha ratio*, which means we apply the estimated alpha ratio for estimating the noise standard deviation.

B. Refining $\sigma_e^{T\alpha}$ and $\sigma_e^{E\alpha}$ to Estimate σ_A

Although $\sigma_e^{T\alpha}$ and $\sigma_e^{E\alpha}$ are closely related to σ_A that we wish to estimate, we do not use them as the direct estimate, but rather we determine how they are related on our training data sets with different levels of synthetically added noise. For all our experiments, we assume that there are $P = 11$ discrete levels of added noise, $\sigma_A \in \{0, 2, 4, \ldots, 20\}$ with the pth value of σ_A given as $2(p-1)$, and with the noise variance ratios for the Canon 10D, $\alpha_R : \alpha_G : \alpha_B = 1.86:0.69:1.0$. Image values are on a scale from 0 to 255. Figure 5(a) shows $\sigma_e^{T\alpha}$ and $\sigma_e^{E\alpha}$ determined as described in Section IV-A along with the true values of σ_A for the 11 added noise levels on a constant image of value 128. There is clearly a linear relationship between σ_A and $\sigma_e^{T\alpha}$, $\sigma_e^{E\alpha}$, and for this image we conclude that $\sigma_A \approx MO^{T\alpha}\sigma_e^{T\alpha} \approx MO^{E\alpha}\sigma_e^{E\alpha}$, where from the graph we identify $MO^{T\alpha} = 1.0265$ and $MO^{E\alpha} = 1.1920$. We note in particular that both methods give an estimate of 0 when no noise is added.
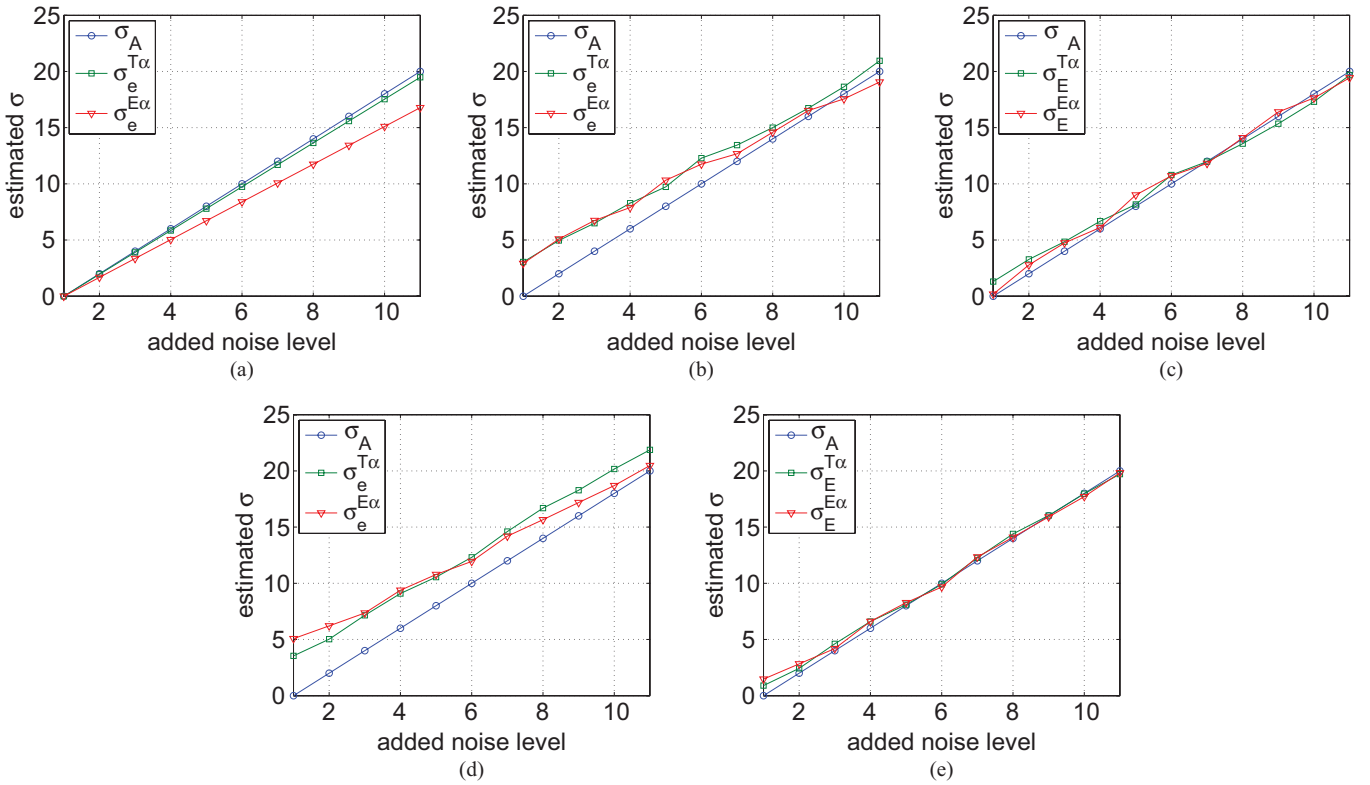
Fig. 5. Estimated quantities as a function of the added noise level. σ_A is shown in all cases. (a) $\sigma_e^{T\alpha}$ and $\sigma_e^{E\alpha}$ estimated from a constant image of value 128. (b) $\sigma_e^{T\alpha}$ and $\sigma_e^{E\alpha}$ estimated from the KO data set. (c) $\sigma_E^{T\alpha}$ and $\sigma_E^{E\alpha}$ estimated from the KO data set with values of MO and AO given in Table I. (d) $\sigma_e^{T\alpha}$ and $\sigma_e^{E\alpha}$ estimated from the LC data set. (f) $\sigma_E^{T\alpha}$ and $\sigma_E^{E\alpha}$ estimated from the LC data set with values of MO and AO given in Table I.

Fig. 5(b) and (d) show the values of $\sigma_e^{T\alpha}$ and $\sigma_e^{E\alpha}$ for the 11 levels of added noise on the KO and LC data sets; estimates were obtained for each image in the data set, and these were averaged. We see a similar slope to that in Fig. 5(a), but also an additive offset due to the underlying noise in these image data sets in addition to the added noise. In our application, we wish to estimate the *added noise*, in order to relate it to the noise level in the training data set with different levels of added noise. Thus we propose estimators of the form

$$\sigma_E^{T\alpha} = MO^{T\alpha} \times \sigma_e^{T\alpha} + AO_{LC}^{T\alpha}, \tag{17}$$
$$\sigma_E^{E\alpha} = MO^{E\alpha} \times \sigma_e^{E\alpha} + AO_{LC}^{E\alpha}. \tag{18}$$

Using the multiplicative factors found above, we determined an additive offset so that the estimates in Eq. (17) and Eq. (18) approximate σ_A as closely as possible over the range of added noise values. The resulting values are shown in Table I and the graphs of $\sigma_E^{T\alpha}$ and $\sigma_E^{E\alpha}$ for the KO and LC data sets are shown in Fig. 5(c) and (e), showing that a good estimate of the parameter σ_A can be obtained over the range of added noise, in both cases where the ratios of noise levels in the different channels are known or unknown. Note that the noise level in the LC data set is a bit higher than in the KO data set, leading to a slightly higher offset.

V. FILTER SET SELECTOR

Our LSLCD-NE design algorithm can be summarized as follows. We first add Gaussian noise with parameter σ_A

TABLE I
ADDITIVE AND MULTIPLICATIVE PARAMETERS FOR ESTIMATE OF σ_E

	MO	AO_{LC}	AO_{KO}
$T\alpha$	1.027	−2.732	−1.825
$E\alpha$	1.192	−4.576	−3.292

(standard deviations $\sqrt{\alpha_R}\sigma_A$, $\sqrt{\alpha_G}\sigma_A$, $\sqrt{\alpha_B}\sigma_A$ in each color channel) to the Bayer CFA images, with $\sigma_A \in \{0, 2, \ldots, 20\}$ as described above. We designed optimal filters for the LSLCD system using the different noise levels in this set (with the method shown in Section III, using the entire data set as training set). We denote the resulting LSLCD demosaicking systems $\mathcal{D}^{(2(p-1))}$. Noise level estimation was introduced in Section IV, where we use $\sigma_E^{T\alpha}$ or $\sigma_E^{E\alpha}$ to estimate σ_A. While the added noise levels σ_A are discrete even numbers, the estimated $\sigma_E^{T\alpha}$ and $\sigma_E^{E\alpha}$ are continuous values. Thus, we have to assign one filter set to the obtained $\sigma_E^{T\alpha}$ or $\sigma_E^{E\alpha}$.

In this section, we show how to do this based on the values of $\sigma_E^{T\alpha}$, i.e., assuming that the ratios of the noise variances in the three channels of the CFA are known. The procedure is the same when using $\sigma_E^{E\alpha}$. For each image $f^{(k)}$ in the training set, and with each level of noise $2(p-1)$, we determined the best filter set by exhaustive search based on the color mean squared error CMSE:

$$BF(k, \sigma_A) = \arg \min_{\sigma \in \{0,2,\ldots,20\}} \text{CMSE} \left(\mathcal{D}^{(\sigma)} f_{\text{CFAN}}^{(k,\sigma_A)}, f^{(k)} \right). \tag{19}$$
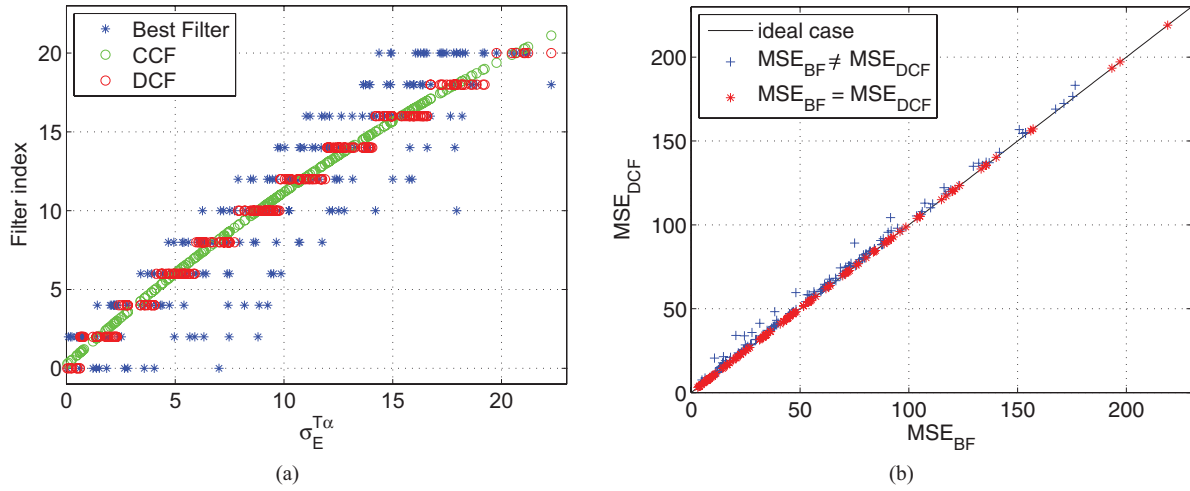
Fig. 6. (a) Scatter plot of best filter index versus $\sigma_E^{T\alpha}$ (blue *), with best quadratic fit (green ∘) CCF and the discrete chosen filter DCF (red ∘). (b) Scatter plot of CMSE obtained with the best filter versus the CMSE with the DCF. Points shown in red have the same CMSE.

We also determine the noise estimate $\sigma_E^{T\alpha}$. Fig. 6(a) shows a scatter plot of the index of the best filter versus $\sigma_E^{T\alpha}$ (blue stars). There is a clear trend, and we fit this data with least-squares polynomials of various order, concluding that a second order polynomial fit was the most appropriate. Fig. 6(a) also shows the least-squares quadratic fit to this data (green circles), denoted *CCF*. As our selected filter, we simply take the nearest even integer,

$$DCF = 2 \times \text{round}\left(\frac{CCF}{2}\right), \qquad (20)$$

shown as red circles in Fig. 6(a). After the training phase, $DCF(\sigma_E^{T\alpha})$ is saved as a quantizer-like function that partitions the $\sigma_E^{T\alpha}$ axis into P disjoint intervals and assigns the value of DCF depending on which interval contains the measured $\sigma_E^{T\alpha}$. The procedure is general and can be applied for any number P of design standard deviations, which could also be non-uniformly distributed.

To evaluate the effectiveness of this procedure, Fig. 6(b) shows for the Kodak image set, a plot of the CMSE obtained with the *DCF* versus the CMSE obtained with the best of the available filters *BF*. Points are red when *DCF* is equal to *BF*. When $DCF \neq BF$, the points are shown in blue. From the result, 40.91% of all cases correctly assigned *DCF* to *BF* for the Kodak image set. It is clear that there is very little difference between use of the filter set obtained by this procedure and use of the best filter set (which is of course unknown in actual use).

VI. EXPERIMENTAL RESULTS

To evaluate the performance of the proposed LSLCD-NE algorithm, we compare it with other algorithms reported in the literature. The performance measurements are CPSNR and S-CIELAB ΔE^* as in previous papers on this topic. For experimental validation, we consider the Kodak test set of 24 color images of size 768×512. We obtained ST (self-trained on the given image) and GT (global-trained on all images) filter sets for 24 Kodak images using the *DCF*

TABLE II

CPSNR RESULTS OF SELECTED DEMOSAICKING ALGORITHMS AND THE PROPOSED LSLCD-NE ALGORITHM WHEN $ANL \in \{1, 2, \ldots, 11\}$. LSLCD EMPLOYED 11×11 SIZED h_{TO} AND LSLCD-NE EMPLOYED 11×11 SIZED h_{GT} WITH σ_A KNOWN

ANL	AHD [3]	LMMSE [4]	RAD [7]	LSLCD [2]	LSLCD-NE
1	37.58	40.10	39.76	40.22	40.26
2	36.27	37.99	37.75	37.96	37.51
3	33.93	34.84	34.63	34.68	34.91
4	31.74	32.22	32.02	32.00	32.90
5	29.87	30.11	29.91	29.85	31.41
6	28.27	28.38	28.18	28.10	30.27
7	26.91	26.93	26.72	26.64	29.37
8	25.71	25.68	25.47	25.38	28.64
9	24.67	24.58	24.38	24.28	28.03
10	23.73	23.62	23.41	23.31	27.51
11	22.89	22.75	22.54	22.44	27.06
avg	29.23	29.75	29.52	29.53	31.62

criterion described above. If $DCF \leq 0$, we assume no noise exists in the CFA image and original LSLCD algorithm is used for demosaicking; in this case, the performance is the same as in [2]. If $DCF > 0$, we apply our proposed LSLCD-NE algorithm.

A. Comparison of Selected Conventional Demosaicking Algorithms With LSLCD-NE

In Tables II and III, we give a CPSNR and S-CIELAB ΔE^* comparison between conventional demosaicking algorithms which do not account for the noise (AHD [3], LMMSE [4], RAD [7], LSLCD [2] with 11×11 h_{TO} filters[1]) and the proposed LSLCD-NE (with 11×11 h_{GT} filters trained on all 24 images, and σ_A known) for different added noise levels (ANL). Here, ANL is an integer from 1 to 11 with corresponding value of σ_A as described in section IV. The LSLCD algorithm shows better performance than the

---

[1]Filter h_{TO} is trained on the other 23 images in the Kodak data set. We assume that h_{TO} is almost identical to h_{GT} as found previously.

TABLE III

S-CIELAB ΔE^* Result of Selected Demosaicking Algorithms and the Proposed LSLCD-NE Algorithm When $ANL \in \{1, 2, \ldots, 11\}$. LSLCD Employed 11×11 Sized f_{TO} and LSLCD-NE Employed 11×11 Sized f_{GT} With σ_A Known

ANL	AHD [3]	LMMSE [4]	RAD [7]	LSLCD [2]	LSLCD-NE
1	0.939	0.787	0.842	0.779	0.776
2	1.180	1.061	1.098	1.068	1.079
3	1.621	1.532	1.583	1.565	1.522
4	2.128	2.061	2.129	2.121	1.972
5	2.664	2.616	2.704	2.705	2.397
6	3.217	3.187	3.295	3.304	2.793
7	3.781	3.768	3.897	3.915	3.163
8	4.352	4.358	4.507	4.533	3.512
9	4.928	4.954	5.123	5.157	3.842
10	5.510	5.556	5.744	5.787	4.157
11	6.094	6.163	6.369	6.421	4.459
avg	3.310	3.277	3.390	3.396	2.697

TABLE IV

Noise Estimation Conditions Evaluated in Fig. 7

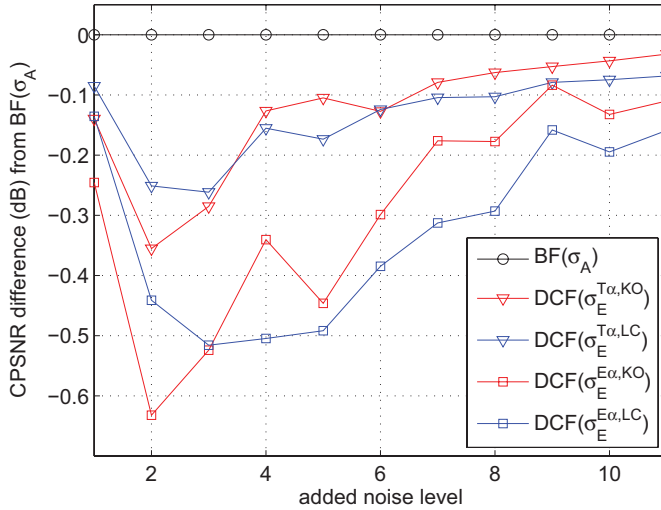| ANL	$\alpha_R : \alpha_G : \alpha_B$ ratio	ImageSet	σ decision
Known	–	–	σ_A
Unknown	known	Kodak	$\sigma_E^{T\alpha, KO}$
Unknown	unknown	Kodak	$\sigma_E^{E\alpha, KO}$
Unknown	known	LC	$\sigma_E^{T\alpha, LC}$
Unknown	unknown	LC	$\sigma_E^{E\alpha, LC}$

Fig. 7.   Comparison of the noise estimation methods.

LSLCD-NE algorithm when $ANL = 2$, and results are comparable when $ANL = 1$. However, the original LSLCD algorithm is seriously affected by noise as ANL increases. The proposed LSLCD-NE with h_{LN} yields better performance when ANL is high, while it is still comparable with LSLCD when ANL is low. LSLCD-NE performs better than all the other methods tested for ANL values of 3 or more with both performance measures.
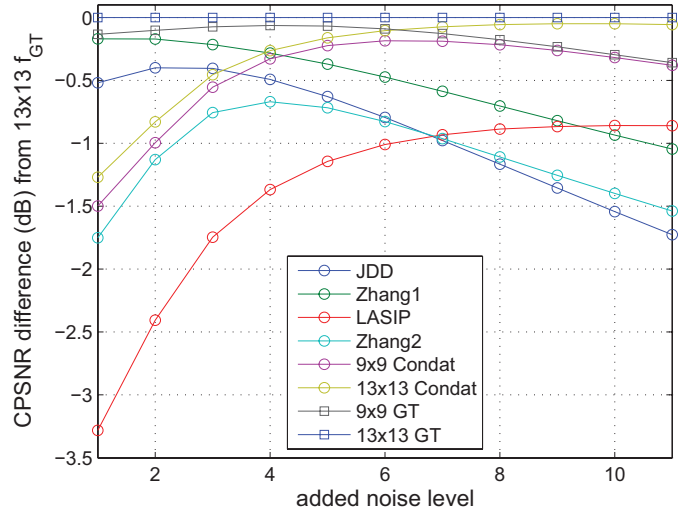

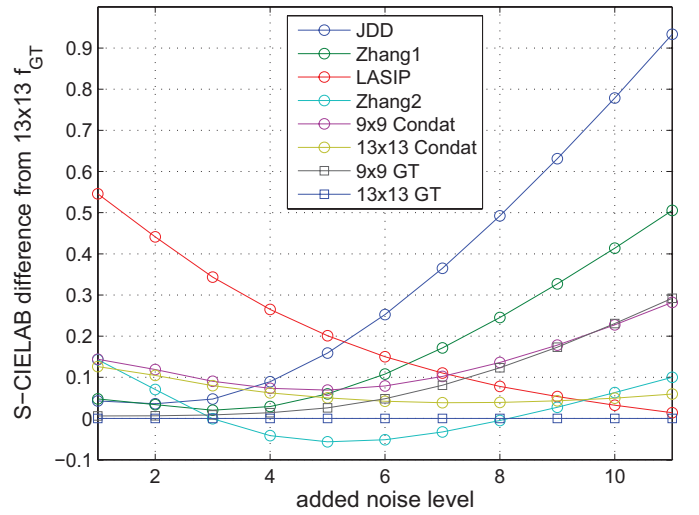Fig. 8.   CPSNR difference from LSLCD-NE with 13×13 sized f_{GT} with conventional joint demosaicking/denoising methods.

Fig. 9.   S-CIELAB ΔE^* difference from LSLCD-NE with 13×13 sized f_{GT} with conventional joint demosaicking/denoising methods.

B. Evaluation of Noise Estimation Schemes

If we know σ_A, we can select the filter corresponding to $BF(\sigma_A)$. However, in most cases σ_A, and perhaps the ratios $\alpha_R : \alpha_G : \alpha_B$ that characterize the image capture, are unknown at the demosaicking step, and thus we have to estimate σ_E and perhaps the α_i. There are four cases for estimating σ_E that we have evaluated, as shown in Table IV. Fig. 7 shows CPSNR results on the Kodak data set when different methods for estimating noise parameters are used compared to when the best filter is used. For this assessment, we used 11×11 self-trained filters. From the figure, we see $BF(\sigma_A)$ gives the best result, followed by $DCF(\sigma_E^{T\alpha, KO})$, $DCF(\sigma_E^{T\alpha, LC})$, $DCF(\sigma_E^{E\alpha, KO})$, and $DCF(\sigma_E^{E\alpha, LC})$ in that order. From this result, we see that the training set has little impact, while knowing the true alpha ratio has somewhat more effect. When CPSNR is plotted, all curves look pretty much the same, demonstrating that our noise estimation is quite effective in the context of LSLCD-NE demosaicking.

TABLE V

CPSNR Performance Comparison for 24 Kodak Data Set When σ_A Is Given. Algorithm Labels (A) JDD [12], (B) Zhang1 [9], (C) LASIP [10], (D) Zhang2 [11], (E) 9×9 Condat [13], (F) 13×13 Condat [13], (G) 5×5 f_{GT}, (H) 7×7 f_{GT}, (I) 9×9 f_{GT}, (J) 11×11 f_{GT}, (K) 13×13 f_{GT}, (L) 15×15 f_{GT}, (M) 11×11 f_{GT}. (G to L): BM3D Is Used for $\widehat{f}_{LN}$ of Fig. 1. (M): h_{LN} Is Used for $\widehat{f}_{LN}$ of Fig. 1)

ANL	A	B	C	D	E	F	G	H	I	J	K	L	M
1	39.77	40.12	37.01	38.54	38.79	39.02	39.10	39.83	40.16	40.26	40.28	40.29	40.26
2	38.17	38.39	36.16	37.44	37.57	37.74	37.66	38.26	38.46	38.54	38.56	38.57	37.51
3	36.07	36.26	34.73	35.72	35.92	36.02	35.73	36.29	36.40	36.45	36.47	36.47	34.91
4	34.32	34.53	33.45	34.15	34.49	34.55	34.04	34.65	34.75	34.79	34.81	34.81	32.90
5	32.90	33.16	32.38	32.81	33.30	33.36	32.64	33.33	33.46	33.50	33.52	33.53	31.41
6	31.71	32.03	31.50	31.68	32.32	32.40	31.47	32.25	32.42	32.47	32.49	32.51	30.27
7	30.70	31.09	30.75	30.71	31.49	31.60	30.48	31.33	31.55	31.64	31.66	31.68	29.37
8	29.82	30.28	30.10	29.88	30.77	30.93	29.62	30.55	30.81	30.93	30.97	30.99	28.64
9	29.04	29.58	29.53	29.14	30.14	30.35	28.87	29.85	30.16	30.32	30.37	30.40	28.03
10	28.34	28.95	29.03	28.49	29.57	29.84	28.21	29.24	29.59	29.79	29.85	29.89	27.51
11	27.71	28.39	28.58	27.90	29.06	29.38	27.61	28.68	29.08	29.30	29.38	29.43	27.06
Avg	32.60	32.98	32.11	32.40	33.04	33.20	32.31	33.12	33.35	33.45	33.49	33.51	31.62

TABLE VI

S-CIELAB ΔE^* Performance Comparison for 24 Kodak Data Set When σ_A Is Given. Algorithm Labels (A) to (M) Correspond to Those Used in Table V

ANL	A	B	C	D	E	F	G	H	I	J	K	L	M
1	0.818	0.823	1.321	0.918	0.919	0.901	0.841	0.807	0.781	0.776	0.775	0.775	0.776
2	1.062	1.060	1.467	1.097	1.145	1.131	1.092	1.052	1.033	1.027	1.026	1.026	1.079
3	1.439	1.412	1.735	1.391	1.483	1.472	1.487	1.418	1.401	1.396	1.393	1.392	1.522
4	1.836	1.776	2.012	1.705	1.820	1.810	1.911	1.789	1.761	1.754	1.749	1.747	1.972
5	2.236	2.136	2.278	2.020	2.146	2.127	2.344	2.153	2.103	2.087	2.080	2.077	2.397
6	2.632	2.488	2.530	2.329	2.459	2.422	2.780	2.510	2.428	2.398	2.386	2.380	2.793
7	3.026	2.832	2.771	2.628	2.763	2.699	3.219	2.861	2.741	2.691	2.671	2.661	3.163
8	3.415	3.168	3.001	2.918	3.059	2.962	3.660	3.208	3.046	2.972	2.939	2.923	3.512
9	3.802	3.498	3.224	3.198	3.349	3.214	4.102	3.551	3.344	3.243	3.196	3.171	3.842
10	4.186	3.821	3.439	3.470	3.635	3.457	4.547	3.892	3.638	3.506	3.442	3.407	4.157
11	4.567	4.140	3.648	3.734	3.916	3.694	4.992	4.232	3.926	3.764	3.682	3.634	4.459
Avg	2.638	2.469	2.493	2.310	2.427	2.353	2.816	2.497	2.382	2.328	2.304	2.290	2.697

TABLE VII

Average Time (s) to Demosaic One 512×768 Image of the Kodak Data Set When σ_A Is Given. Algorithm Labels (A) to (M) Correspond to Those Used in Table V

	A	B	C	D	E	F	G	H	I	J	K	L	M
Time/image	4.975	72.679	6.672	289.809	9.221	9.566	9.359	9.420	9.397	9.430	9.537	9.419	0.942

C. Comparison of LSLCD-NE With Other Joint Demosaicking/Denoising Systems

Tables V and VI show CPSNR and S-CIELAB ΔE^* performance of several versions of the proposed algorithm and other joint demosaicking/denoising systems from the literature, as described in the introduction. Figures 8 and 9 graphically show the performance difference between one reference implementation of LSLCD-NE (K in the tables) and these same methods. In all cases the noise level σ_A and the noise variance ratios are assumed known, since the methods from the literature do not incorporate noise estimation. However, the other methods do not make use of the noise variance ratios. Readers can make a subjective performance comparison by

viewing selected demosaicked images at the companion web site [21]. Some closeups of selected critical areas are also shown, as well as results for a few other images outside the Kodak data set.

As a first observation, we note that the proposed method outperforms all the other methods over the entire range of noise levels in terms of CPSNR. For the S-CIELAB ΔE^* measure, the method noted D: Zhang2 performed slightly better for added noise levels from 4 to 8. The methods E and F of Condat perform very similarly to the proposed method at higher noise levels, while the methods A: JDD and B: Zhang1 perform well at lower noise levels. Fig. 10 illustrates the performance of LSLCD-NE at the highest added noise level (ANL = 11, $\sigma_A = 20$) in comparison with two other methods

Fig. 10. Results on zoomed-in portion of Kodak image 8 with ANL = 11 ($\sigma_A = 20$). (a) Original. (b) LSLCD-NE. (c) Zhang2. (d) 13×13 Condat.

on a zoomed portion of Kodak image 8. The comparison methods are the closest comptetitors, Zhang2 (D) and 13×13 Condat (F). On this region, we see that LSLCD-NE gives a more pleasing reproduced image than method D, and has better color crosstalk suppression than method F. Again, many more results can be found on the companion web site [21].

Regarding the proposed LSLCD-NE method, we have used filter sizes ranging from 5×5 to 15×15 (G-L), allowing a tradeoff between complexity and demosaicking performance. It is clear that we can do better than 5×5, but gains above 11×11 are getting small. Method M shows the result of using a least-squares filter for the luma component rather than the BM3D filter. This clearly degrades the performance and is not as good as any of the competing methods, so use of the BM3D filter is definitely preferred.

Table VII shows the average time in seconds to demosaic one 512×768 image of the Kodak data set. From the result we see filter size does not seriously affect the computation time. We see that the BM3D filter for the luma chroma contributes significantly to the complexity, but it is needed to get suitable performance. All methods from the literature were tested using the software made available by the authors of these methods on their web sites. Although these times

are only a rough measure of complexity, they do give important information on the relative complexity of the different methods.

VII. Conclusion

This paper has extended the adaptive luma-chroma demultiplexing algorithm of [2] to noisy CFA images, taking into account the different noise levels in the different color channels, and providing a noise-level estimation scheme. The resulting method shows that LSLCD is an algorithm of choice for noisy CFA demosaicking, and performs very well at all noise levels with a very competitive level of complexity. This is the only method we have seen that explicitly accounts for different noise levels in the different channels in designing the demosaicking algorithm. The methods proposed are general and can be applied to other CFA designs than the Bayer, including those with more than 3 types of color filters, and other noise models. For example, some CFA designs use a panchromatic channel to improve noise performance, and the proposed algorithm can be adapted to exploit this feature as much as possible. It would also be interesting to combine the LSLCD method with modern, locally adaptive denoising schemes to get better overall performance.

Many results are provided on our companion web site along with software to reproduce our results.

REFERENCES

[1] D. Menon and G. Calvagno, "Color image demosaicking: An overview," *Signal Process. Image Commun.*, vol. 26, nos. 8–9, pp. 518–533, 2011.

[2] B. Leung, G. Jeon, and E. Dubois, "Least-squares luma–chroma demultiplexing algorithm for Bayer demosaicking," *IEEE Trans. Image Process.*, vol. 20, no. 7, pp. 1885–1894, Jul. 2011.

[3] K. Hirakawa and T. W. Parks, "Adaptive homogeneity-directed demosaicking algorithm," *IEEE Trans. Image Process.*, vol. 14, no. 3, pp. 360–369, Mar. 2005.

[4] L. Zhang and X. Wu, "Color demosaicking via directional linear minimum mean square-error estimation," *IEEE Trans. Image Process.*, vol. 14, no. 12, pp. 2167–2177, Dec. 2005.

[5] E. Dubois, "Frequency-domain methods for demosaicking of Bayer-sampled color image," *IEEE Signal Process. Lett.*, vol. 12, no. 12, pp. 847–850, Dec. 2005.

[6] E. Dubois, "Filter design for adaptive frequency-domain Bayer demosaicking," in *Proc. IEEE Int. Conf. Image Process.*, Oct. 2006, pp. 2705–2708.

[7] D. Menon and G. Calvagno, "Regularization approaches to demosaicking," *IEEE Trans. Image Process.*, vol. 18, no. 10, pp. 2209–2220, Oct. 2009.

[8] K. Hirakawa and T. W. Parks, "Joint demosaicking and denoising," *IEEE Trans. Image Process.*, vol. 15, no. 8, pp. 2146–2157, Aug. 2006.

[9] L. Zhang, X. Wu, and D. Zhang, "Color reproduction from noisy CFA data of single sensor digital cameras," *IEEE Trans. Image Process.*, vol. 16, no. 9, pp. 2184–2197, Sep. 2007.

[10] D. Paliy, V. Katkovnik, R. Bilcu, S. Alenius, and K. Egiazarian, "Spatially adaptive color filter array interpolation for noiseless and noisy data," *Int. J. Imag. Syst. Technol.*, vol. 17, no. 3, pp. 105–122, Oct. 2007.

[11] L. Zhang, R. Lukac, X. Wu, and D. Zhang, "PCA-based spatially adaptive denoising of CFA images for single-sensor digital cameras," *IEEE Trans. Image Process.*, vol. 18, no. 4, pp. 797–812, Apr. 2009.

[12] D. Menon and G. Calvagno, "Joint demosaicking and denoising with space-varying filters," in *Proc. IEEE Int. Conf. Image Process.*, Nov. 2009, pp. 477–480.

[13] L. Condat, "A new color filter array with optimal properties for noiseless and noisy color image acquisition," *IEEE Trans. Image Process.*, vol. 20, no. 8, pp. 2200–2210, Aug. 2011.

[14] S. H. Park, H. S. Kim, S. Lansel, M. Parmar, and B. A. Wandell, "A case for denoising before demosaicking color filter array data," in *Proc. Conf. Record 43rd Asilomar Signals Syst. Comput.*, 2009, pp. 860–864.

[15] A. Danielyan, M. Vehvilainen, A. Foi, V. Katkovnik, and K. Egiazarian, "Cross-color BM3D filtering of noisy raw data," in *Proc. Int. Workshop Local Non-Local Approx. Image Process.*, Aug. 2009, pp. 125–129.

[16] K. Hirakawa, X.-L. Meng, and P. J. Wolfe, "A framework for wavelet-based analysis and processing of color filter array images with applications to denoising and demosaicking," in *Proc. IEEE Int. Conf. Acoustics Speech Signal Process.*, Apr. 2007, pp. 597–600.

[17] G. E. Healey and R. Kondepudy, "Radiometric CCD camera calibration and noise estimation," *IEEE Trans. Pattern Anal. Mach. Intell.*, vol. 16, no. 3, pp. 267–276, Mar. 1994.

[18] J. E. Adams, J. F. Hamilton, M. Kumar, E. O. Morales, R. Palum, and B. H. Pillman, "Single capture image fusion," in *Computational Photography: Methods and Applications*, R. Lukac, Ed. Boca Raton, FL: CRC Press, 2010, pp. 1–62.

[19] K. Dabov, A. Foi, V. Katkovnik, and K. Egiazarian, "Image denoising by sparse 3-D transform-domain collaborative filtering," *IEEE Trans. Image Process.*, vol. 16, no. 8, pp. 2080–2095, Aug. 2007.

[20] A. Amer and E. Dubois, "Fast and reliable structure-oriented video noise estimation," *IEEE Trans. Trans. Circuits Syst. Video Technol.*, vol. 15, no. 1, pp. 113–118, Jan. 2005.

[21] E. Dubois and G. Jeon. (2011). *Demosaicking of Noisy Bayer-Sampled Color Images with Least-Squares Luma-Chroma Demultiplexing and Noise Level Estimation: Additional Results* [Online]. Available: http://www.site.uottawa.ca/~edubois/lslcd_ne/

[22] E. Dubois, "Color filter array sampling of color images: Frequency-domain analysis and associated demosaicking algorithms," in *Single Sensor Imaging: Methods and Applications for Digital Cameras*, R. Lukac, Ed. Boca Raton, FL: CRC Press, 2009, pp. 183–212.

[23] D. Eric, *The Structure and Properties of Color Spaces and the Representation of Color Images*. San Rafael, CA: Morgan and Claypool, 2010.

[24] A. Foi, M. Trimeche, V. Katkovnik, and K. Egiazarian, "Practical Poissonian–Gaussian noise modeling and fitting for single-image raw-data," *IEEE Trans. Image Process.*, vol. 17, no. 10, pp. 1737–1754, Oct. 2008.

[25] C. P. Huynh and A. Robles-Kelly, "Comparative colorimetric simulation and evaluation of digital cameras using spectroscopy data," in *Proc. 9th Biennial Conf. Australian Pattern Recogn. Soc. Digital Image Comput. Tech. Appl.*, 2007, pp. 309–316.

[26] C. Poynton, "Perceptual uniformity in digital imaging," in *Proc. Gjøvik Color Imag. Symp.*, 2009, pp. 102–109.

[27] L. Condat. (2011). *Welcome to Laurent Condat's Image Database* [Online]. Available: http://www.greyc.ensicaen.fr/~lcondat/imagebase.html

Gwanggil Jeon (S'06–M'08) received the B.S., M.S., and Ph.D. (*summa cum laude*) degrees from the Department of Electronics and Computer Engineering, Hanyang University, Seoul, Korea, in 2003, 2005, and 2008, respectively.

He was with the Department of Electronics and Computer Engineering, Hanyang University, from 2008 to 2009. He was with the School of Information Technology and Engineering, University of Ottawa, Ottawa, ON, Canada, as a Post-Doctoral Fellow, from 2009 to 2011. He was with the Graduate School of Science and Technology, Niigata University, Niigata, Japan, as an Assistant Professor, from 2011 to 2012. He is currently an Assistant Professor with the Department of Embedded Systems Engineering, University of Incheon, Incheon, Korea. His current research interests include image processing, particularly image compression, motion estimation, demosaicking, and image enhancement, and computational intelligence, such as fuzzy and rough sets theories.

Dr. Jeon was a recipient of the IEEE Chester Sall Award in 2007 and the ETRI Journal Paper Award in 2008.

Eric Dubois (S'72–M'77–SM'85–F'96) received the B.Eng. (Hons.) degree with great distinction and the M.Eng. degree from McGill University, Montreal, QC, Canada, in 1972 and 1974, respectively, and the Ph.D. degree from the University of Toronto, Toronto, ON, Canada, in 1978, all in electrical engineering.

He was a Professor with the INRS Télécommunications Centre, Institut National de la Recherché Scientifique, University of Quebec, Montreal, from 1977 to 1998. Since 1998, he has been a Professor with the School of Information Technology and Engineering (SITE), University of Ottawa, Ottawa, ON, where he was the Vice-Dean of Research and the Secretary of the Faculty of Engineering from 2001 to 2004, and was the Director of SITE from 2006 to 2008. He is involved in research on compression and processing of still and moving images, and multidimensional digital signal processing theory. His current research interests include stereoscopic and multiview imaging, image sampling theory, image-based virtual environments, and color signal processing. His research is carried out in collaboration with organizations such as the Communications Research Centre, the National Research Council, the RCMP, and the Learning Objects Repositories Network.

Dr. Dubois was a co-recipient of the Journal Award from the Society of Motion Picture and Television Engineers in 1988. He is a fellow of the Canadian Academy of Engineering and the Engineering Institute of Canada. He is a registered Professional Engineer in Quebec, as a member of the Order of Engineers of Quebec. He is a member of the Society for Information Display and the Society for Imaging Science and Technology. He is an Editorial Board Member of the EURASIP journal *Signal Processing: Image Communication* and was an Associate Editor of the IEEE TRANSACTIONS ON IMAGE PROCESSING from 1994 to 1998. He was a Technical Program Co-Chair of the IEEE International Conference on Image Processing in 2000 and a member of the Organizing Committee of the IEEE International Conference on Acoustics, Speech, and Signal Processing in 2004.